**555.        A Hybrid Nudging-Ensemble Kalman Filter Approach to Data Assimilation in WRF/DART**

Lili Lei and David R. Stauffer*
Pennsylvania State University, University Park, PA

## 1. Introduction

A hybrid nudging-EnKF (HNEnKF) approach has been developed and tested in the Lorenz three-variable model (Lei et al. 2011a) and a two-dimensional (2D) shallow water model (Lei et al. 2011b) for dynamic analysis and numerical weather prediction. In this paper it is applied to a three-dimensional mesoscale model using real data.

The HNEnKF combines the EnKF (Evensen 1994; Houtekamer and Mitchell 1998) and observation nudging (Stauffer and Seaman 1990; Stauffer and Seaman 1994) to take advantage of the strengths of both methods while avoiding their individual weaknesses. It applies the EnKF gradually in time via nudging-type terms to achieve better temporal smoothness and inter-variable consistency and reduce the data insertion shocks that often occur with intermittent data assimilation methods. The HNEnKF uses flow-dependent and time-dependent hybrid nudging coefficients based on the gain matrix of the EnKF rather than ad-hoc nudging coefficients based largely on past experience (e.g., Stauffer and Seaman 1994; Schroeder et al. 2006). It also extends the traditional observation nudging coefficients (Stauffer and Seaman 1994) to include zero off-diagonal elements in the nudging magnitude matrix to improve the inter-variable influences of the innovations and the dynamic consistency.

Building on the idealized model results using observing system simulation experiments (OSSEs) in Lei et al. (2011a, b), we apply the HNEnKF to real surface and rawinsonde data in the three-dimensional Weather Research and Forecast (WRF) model (Skamarock et al. 2008). The EnKF and HNEnKF calculations are performed within the Data Assimilation Research Testbed (DART, Anderson et al. 2009). As in our previous papers, the HNEnKF is again compared to the EnKF and nudging applied separately, but here we perform a real-data study with truly independent verification of the data assimilation results against surface tracer data.

A 48-h simulation of the Cross Appalachian Tracer Experiment (CAPTEX-83, Deng et al. 2004) case from 1200 UTC 18 September 1983 to 1200 UTC 20 September 1983 is conducted. Both surface and rawinsonde observations are assimilated. The hourly meteorological outputs are then used to drive the Second-Order Closure Integrated Puff (SCIPUFF, Sykes et al. 2004) atmospheric transport and dispersion (AT&D) model. The observed surface tracer concentration data is then used as an independent verification of the data assimilation approaches. The SCIPUFF-predicted surface tracer concentrations driven

*Corresponding author: David R. Stauffer, 621 Walker Building, University Park, PA 16802, USA, stauffer@meteo.psu.edu, 814-863-3932.

by the hourly dynamic analyses from the set of data assimilation experiments are compared statistically to the observed surface tracer data.

In section 2, the methodology of the HNEnKF approach is briefly described. Section 3 presents the details of the experiment design, including description of the model, observations, and the parameters used in the data assimilation experiments. An overview of the CAPTEX case and tracer study is presented in section 4. Section 5 discusses the results from the different data assimilation experiments for the meteorology, insertion noise and surface tracer verification. The conclusions of the study are summarized in section 6.

## 2. Methodology for the HNEnKF approach in WRF/DART

The procedures of the HNEnKF approach follow Lei et al. (2011b). A schematic of the HNEnKF approach is shown in Fig. 1. We start with an ensemble of N background forecasts that will be updated by the EnKF (called the "ensemble state"), and a single forecast that will be updated by the hybrid nudging-type terms (called the "nudging state"). The following five steps are repeated for each data assimilation cycle: 1) Compute the hybrid nudging coefficients using the ensemble forecast via the EnKF algorithm. 2) Integrate the nudging state by continuously applying nudging with the hybrid nudging coefficients. 3) Update each ensemble member of the ensemble state using the EnKF. 4) Re-define the ensemble mean to be the analysis of the nudging state by re-centering the ensemble around the nudging state at the observation time while retaining the ensemble spread. 5) Integrate the ensemble state and the nudging state forward to the next observation time.

Equation (1) shows the full set of model equations having the additional nudging terms that are used to gradually relax the model state towards the observation state.

$$\frac{d\mathbf{x}}{dt} = f(\mathbf{x}) + \mathbf{G} \cdot \mathrm{w}_s \cdot \mathrm{w}_t \cdot (\mathbf{x}^o - \mathbf{x}), \qquad (1)$$

where $\mathbf{x}$ and $f$ are the state vector and standard forcing function of the system, $\mathbf{x}^o$ is the observation vector, $\mathbf{G}$ is the nudging magnitude matrix, and $\mathrm{w}_s$ and $\mathrm{w}_t$ are the spatial and temporal nudging weighting coefficients. The spatial and temporal nudging weighting coefficients are used to map the innovation in observation space and time to the model grid cell and time step. The product of $\mathbf{G}$, $\mathrm{w}_s$ and $\mathrm{w}_t$ is defined here as the nudging coefficient. While the $\mathrm{w}_s$ in the shallow water model in Lei et al. (2011b) was two-dimensional (i.e., no vertical dimension), the $\mathrm{w}_s$ in WRF is three-dimensional with variations in both the horizontal and vertical directions.

The flow-dependent hybrid nudging coefficients used in the HNEnKF approach are computed from the ensemble forecast, and are elements of the EnKF gain matrix normalized by the sum of the temporal nudging weighting coefficient over half of the assimilation time window. The flow-dependent hybrid nudging coefficient is then described by Eq. (2):

$$\mathbf{G} \cdot \mathrm{w}_s = \frac{1}{\left( \sum_{t=t^o-\tau_{\mathrm{N}}}^{t^o} \mathrm{w}_t \cdot \Delta t \right)} \cdot \mathbf{K} , \qquad (2)$$

where $\mathbf{K}$ is the EnKF gain matrix, $\Delta t$ is the time step, $t$ is the model time, $t^o$ is the observation time, and $\tau_{\mathrm{N}}$ is the half-period of the nudging time window. The temporal nudging weighting coefficient $\mathrm{w}_t$ follows the trapezoidal function defined by Stauffer and Seaman (1990).

It is important to note that the hybrid nudging coefficients are computed from Eq. (2); that is, they come directly from the EnKF that contains information from the flow-dependent background error covariances. Thus there is no need to specify the nudging strength (i.e., elements in the nudging magnitude matrix $\mathbf{G}$) or the spatial nudging weighting coefficient $\mathrm{w}_s$ in either the horizontal or vertical directions. Substituting the state vector $\mathbf{x}$ by a vector comprised of u- and v- wind components, potential temperature and mixing ratio on every model grid point, Eq. (1) becomes the governing equations of WRF including the hybrid nudging terms with their coefficients defined by Eq. (2). It is also important to note that the hybrid nudging terms include not only the standard diagonal terms (i.e., the innovations in u in the u-equation, and the innovations in v in the v-equation, etc.), but also the off-diagonal terms (i.e., innovations in u in the v-equation, and the innovations in v in the u-equation, etc.). This statistical inter-variable influence of the innovations from the EnKF is included in the model's dynamic relaxation terms to gradually and continuously force the model towards the observations, thereby reducing the error spikes and dynamic imbalances often produced by intermittent assimilation methods (e.g., Lei et al. 2011a, b).

## 3. Model configurations and experiment design
### 3.1 WRF/DART model description

In this study, the WRF-ARW version 3.1.1 (Skamarock et al. 2008) is used to test the HNEnKF approach. The model simulation has horizontal grid-spacing of 12 km on a 208×190 horizontal grid with 33 vertical levels and a model top at 100 hPa. The WRF model domain is shown in Fig. 2. The model is configured to use the longwave Rapid Radiative Transfer Model (RRTM: Mlawer et al. 1997), the shortwave Dudhia radiation scheme (Dudhia 1989), and the thermal diffusion land-surface scheme. Several options are used for model microphysics, convective parameterization and planetary boundary layer (PBL) turbulence, as outlined in Table 1, and discussed in section 3.3.

The simulation starts at 1200 UCT 18 September 1983, and continues for 48 hours. The NCEP / NCAR Global Reanalyses are used to generate the initial conditions (ICs) and lateral boundary conditions (LBCs) for the WRF model. Because the NCEP / NCAR Global Reanalyses have a coarse resolution of 2.5°×2.5°, the ICs and LBCs generated by the reanalyses are enhanced by a modified Cressman objective analysis (Benjamin and Seaman 1985) within a new code called OBSGRID in the WRF Pre-processing System (WPS).

The DART (Anderson et al. 2009) is used to perform the data assimilation calculations of the EnKF, and it is able to interface directly with WRF. The DART has a variety of algorithms for the ensemble filters, such as ensemble adjustment Kalman filter (EAKF; Anderson 2001), ensemble Kalman filter with perturbed observations (Evensen 1994), and particle filter (Snyder et al. 2008), to name a few. The EAKF, the default filter in DART, is chosen here. The EAKF is a deterministic ensemble square root filter, which updates the probability distribution of a model state given the prior estimate of the model state's probability distribution, the observations and their associated errors. The prior probability distribution of the model state is obtained from the statistics of an ensemble that incorporates flow-dependent background error covariance information. For simplicity, the EAKF is called EnKF in the following discussions, since the EAKF is one kind of EnKF. We also modified the WRF/DART code to apply the new HNEnKF approach.

### 3.2 Observations and verification techniques

Three-hourly WMO surface observations and twelve-hourly rawinsonde observations are assimilated from 1200 UTC 18 September 1983 to 1200 UTC 20 September 1983. For the ensemble-based experiments, the observation error variances of wind and temperature are adapted from WRF 3DVAR (Baker et al. 2004). The observation error variance for relative humidity is set to 10% of the saturated specific humidity.

Ideally we would want to withhold some of the observations for independent verification of the data assimilation methods. However, this case had no special additional meteorological observations. Thus to evaluate and compare the different data assimilation methods on the meteorology, the analysis closeness-of-fit statistics (posteriors) to the assimilated observations are first computed. Then three-hourly forecasts (priors) of each data assimilation method are verified against the observations that will be assimilated during the next data assimilation cycle.

Moreover, an independent verification of the data assimilation approaches is performed by using the hourly WRF experiment outputs in the SCIPUFF AT&D model (Sykes et al. 2004) to predict surface tracer concentrations and then verify them against the observed surface tracer concentration data. In this way, the quality of the analyses produced by each data assimilation method is assessed using the SCIPUFF predictions. The 12-km SCIPUFF domain is shown as the inner black frame within the 12-km WRF domain in

2

Fig. 2. The SCIPUFF simulation starts at 1700 UTC 18 September 1983, and continues for 24 hours. The observed surface tracer concentration data is available at 2200 UTC 18 September 1983, 0400 UTC 19 September 1983, 1000 UTC 19 September 1983, and 16 UTC 19 September 1983. The surface tracer sampling sites and the measurements at 2200 UTC 18 September 1983 are shown in Fig. 3.

### 3.3 Ensemble configurations

Two types of ensembles are configured for the ensemble-based data assimilation experiments. The first ensemble, which is called the IC ensemble, is produced by adding perturbations to the ICs and LBCs interpolated from the NCEP / NCAR global reanalyses and enhanced by OBSGRID. The perturbations are drawn from a multivariate normal distribution by use of the WRF-3DVAR (Baker et al. 2004). This ensemble uses the first model physics configuration in Table 1: the WSM 3-class microphysics scheme (Hong et al. 2004), the Kain-Fritsch cumulus parameterization scheme (Kain and Fritsch 1990) and the Mellor-Yamada_Janjić (MYJ) turbulent kinetic energy (TKE) PBL scheme (Janjić 1994). This type of ensemble is then constructed using both 24 and 48 members.

The second type of ensemble also explores the sensitivities of the ensemble-based data assimilation methods to the physics (PH) configuration, and it is called the ICPH ensemble. The eight different physics configurations shown in Table 1 are applied. Besides the physics schemes used in the IC ensemble, the Lin et al. microphysics scheme (Lin et al. 1983), Betts-Miller-Janjić convective scheme (Betts and Miller 1986; Janjić 1994), and the Yonsei University (YSU) PBL scheme (Hong et al. 2006) are also used. Three IC ensemble members are generated the same way as in the IC ensemble for each physics configuration to produce the 24-member ICPH ensemble. For the 48-member ICPH ensemble, six IC ensemble members are generated the same way as in the IC ensemble for each of the eight physics configurations.

### 3.4 Experiment design

The complete set of data assimilation experiments is defined in Table 2. Experiment CTRL has no data assimilation throughout the 48-h period. The FDDA experiment uses observation nudging (Stauffer and Seaman 1994; Deng et al. 2009) throughout the WRF simulation period to gradually relax the model state u-component and v-component winds, potential temperature and mixing ratio towards the observations. The major parameters used by FDDA are summarized in Table 3. The nudging strength is specified to be $4 \times 10^{-4}$ s$^{-1}$. Standard spatial and temporal weighting functions (Stauffer and Seaman 1994; Schroeder et al. 2006) are used for the observation nudging. The horizontal radius of influence varies from 67 km at the surface, to 100 km above the surface, to 200 km at 500 hPa and levels higher than 500 hPa (Schroeder et al. 2006). The horizontal weighting function also varies

with the difference between terrain elevation at the observation site and that at the surrounding grid points (e.g, Stauffer and Seaman 1994). The vertical weighting function used to spread surface data above the surface follows Rogers et al. (2011). For the stable PBL model regimes, the vertical weighting function is 1.0 from surface to 50 m above ground level (AGL), and then it linearly decreases to 0.0 from 50 m to 100 m AGL. For the unstable PBL regimes, the vertical weighting function is 1.0 from the surface through the model PBL depth, and then it linearly decreases to 0.0 from the PBL top to 50 m above the PBL top. The half-period of the time window is 1 hour for the surface data and 2 hours for the rawinsonde data.

The EnKF experiments use the default EnKF in DART to assimilate the wind, temperature and mixing ratio observations. Experiments EnKFIC24 and EnKFIC48 use the 24-member and 48-member IC ensembles, respectively. Experiments EnKFICPH24 and EnKFICPH48 use the 24-member and 48-member ICPH ensembles, respectively. The HEnKF experiments are single-model experiments that use the HNEnKF approach to assimilate the wind, temperature and mixing ratio observations. The HEnKFIC24 and HEnKFIC48 use the 24-member and 48-member IC ensemble, and HEnKFICPH24 and HEnKFICPH48 use the the 24-member and 48-member ICPH ensemble.

The major data assimilation parameters for Experiments EnKF and HEnKF are also summarized in Table 3. As discussed above, the hybrid nudging coefficients of HEnKF, which are the product of **G** and $W_s$, are computed directly from the EnKF; thus there is no need to specify the nudging strength and spatial weighting function for the HEnKF. The half-period nudging time window of HEnKF is specified the same as that in the FDDA. Both the EnKF and HEnKF experiments use error covariance localization to avoid the unrealistic error correlations at larger distance scales and filter divergence. The ensemble error covariance localization is applied following Gaspari and Cohn (1999). A fifth-order correlation function is performed in the three-dimensional physical space. Two parameters, one for the horizontal cutoff distance and the other for the vertical cutoff distance, are used to control the error covariance localization scale. The horizontal cutoff distance is defined to be 533 km, which is the same radius as the first scan used in the modified Cressman objective analysis in OBSGRID based on the rawinsonde spacing in the United States. The vertical cutoff distance is set to 150 hPa. Finally, adaptive error covariance inflation (Anderson 2007) is also used to reduce filter error and avoid filter divergence for the ensemble-based data assimilation experiments. The values of the adaptive error covariance inflation are computed by using a hierarchical Bayesian approach and the same assimilated observations.

### 4. The CAPTEX-83 case

The 18-20 September 1983 episode from CAPTEX is chosen as the test case for the HNEnKF in WRF/DART. This mid-latitude cyclone case is widely

used for air-quality and regional transport studies (e.g., Deng et al. 2004; Deng and Stauffer 2006). This case initially features a large anticyclone centered over the Mid-Atlantic coast. To the northwest of the high pressure system, a cold front and a warm front propagated quickly through the western Great Lakes with areas of showers and thunderstorms varying in intensity and location through the period. The locations of the fronts at 2200 UTC 18 September are shown in Fig. 3, along with the surface tracer network measurements at this time. The cold front is especially important since it tends to define the western edge of the tracer plume through the period.

For this 18-19 September 1983 episode, 208 kg of the perfluorocarbon tracer gas ($C_7F_{14}$) were released at ground level at the release site Dayton, Ohio, denoted by R in Fig. 3. The release period was 1700-2000 UTC 18 September. The tracer cloud reached the lower Great Lakes by 0000 UTC 19 September. By 1200 UTC 19 September, the cold front had decelerated and began to push into northern New York from Lake Ontario. By 0000 UTC 20 September, the cold front pushed eastward into central Maine. The tracer release moved northward and eastward ahead of the advancing cold front.

## 5. WRF/DART Results

In this section, we first perform a statistical evaluation of the dynamic analyses and three-hourly forecasts produced by the set of data assimilation experiments (Table 2) using the meteorological data for wind speed, wind direction, temperature and relative humidity. Then we assess the results of the various data assimilation methods for temporal smoothness and the creation of insertion noise within the model. Finally, we perform an independent verification of the dynamic analyses using the AT&D model and the observed surface concentration tracer data.

### 5.1 Evaluation using meteorological data

The dynamic analyses created by the set of data assimilation experiments for the CAPTEX case use standard three-hourly surface data and twelve-hourly rawinsonde data. The fit-to-observation statistics (posteriors) at each analysis time will be discussed first. Then the three-hourly forecasts (priors) launched from each analysis following data assimilation will be verified against the observations available for the next three-hour cycle of data assimilation. Examination of the priors will indicate the ability of the model to retain the assimilated information from the previous cycle.

Figure 4 shows the average RMS errors of the posteriors for the set of experiments for all layers over the 48-h period for wind speed, wind direction, temperature and relative humidity. All data assimilation experiments produce smaller average RMS errors for the posteriors than the CTRL. Note that Experiments CRTL and FDDA do not use an ensemble and thus their statistics are the same for each ensemble group. For the IC24 experiments (IC ensemble with 24 members),

Experiment FDDA has the smallest RMS errors for all four variables; that is, the WRF simulation using observation nudging FDDA shows the closest fit to the assimilated observations of all the experiments. The HEnKFIC24 has larger RMS errors than the FDDA, but smaller RMS errors than the EnKFIC24 for wind speed, wind direction, temperature and relative humidity. Thus the HEnKFIC24 improves the fit-to-observation statistics compared to the EnKFIC24, although it has larger RMS errors compared to the FDDA.

The average RMS errors of the posteriors for the experiments including multi-physics ensemble members are shown by the group ICPH24 in Fig. 4. For the wind speed and wind direction, the FDDA has the smallest average RMS errors, and the HEnKFICPH24 has lower average RMS errors than those of the EnKFICPH24. For the temperature and relative humidity, the EnKFICPH24 has similar average RMS errors to the FDDA, and both the FDDA and EnKFICPH24 have lower average RMS errors than the HEnKFICPH24.

Comparing the average RMS errors of the group ICPH24 to the group of IC24, we see that EnKFICPH24 and HEnKFICPH24 have similar average RMS errors for wind speed and wind direction to the EnKFIC24 and HEnKFIC24, respectively. For temperature and relative humidity, the EnKFICPH24 and HEnKFICPH24 have smaller RMS errors than the respective IC ensemble experiments, and the reduction of the average RMS error of the EnKFICPH24 is larger than that of the HEnKFICPH24. Thus the addition of the multi-physics ensemble members in the ICPH ensemble improves the fit-to-observation statistics for the mass fields in the EnKF and HEnKF compared to the IC ensemble, and especially so for the EnKF.

The average RMS errors of the posteriors of the experiments with the increased ensemble size of 48 members are shown by the groups IC48 and ICPH48 in Fig. 4. The relative results comparing EnKF and HEnKF are very similar to those reported using the 24 ensemble members. The HEnKF has an advantage in the fit-to-observations over the EnKF, and the inclusion of the multi-physics ensemble members improves the posteriors of the mass fields in both EnKF and HEnKF, with a larger improvement in the EnKF. The increase of ensemble size from 24 to 48 slightly improves the average RMS errors of the EnKF and HEnKF for both the IC and ICPH ensembles.

Figure 5 shows the average RMS errors of the priors of the set of experiments for wind speed, wind direction, temperature and relative humidity. All data assimilation experiments produce smaller average RMS errors in the priors than the CTRL, except for the wind direction priors of the EnKF experiments. For the IC24 group of experiments, the three data assimilation experiments produce very similar average RMS errors for wind speed. The HEnKFIC24 and FDDA have slightly smaller average RMS errors of wind direction than the CTRL, and the EnKFIC24 has even larger average RMS error of wind direction than the CTRL. The HEnKFIC24 and EnKFIC24 have similar average RMS errors for temperature, and they both have smaller average temperature RMS errors than the FDDA. The

4

HEnKFIC24 has smaller average RMS errors of relative humidity than both EnKFIC24 and FDDA. Therefore, the HEnKFIC24 produces similar or better three-hourly forecasts than EnKFIC24 for the wind and mass fields. The HEnKFIC24 also improves the three-hourly forecast of the mass fields compared to the FDDA, and has similar RMS errors to the FDDA for the wind field.

For the group of ICPH24 experiments, the comparisons among the three data assimilation experiments of the average wind speed and wind direction RMS errors are consistent with those from the group of IC24 experiments. For the mass fields, the EnKFICPH24 has slightly smaller average RMS errors than the HEnKFICPH24, while both of them have smaller average RMS errors than the FDDA. Compared to the IC ensemble, the addition of multi-physics ensemble members in the ICPH ensemble slightly improves the three-hourly forecast of the temperature and relative humidity of the EnKF, and the EnKF forecasts for the mass fields are improved compared to the HEnKF, which is consistent with the posteriors.

When the ensemble size increases from 24 to 48 members, the comparative results of the priors from the 48 ensemble member experiments are generally the same as those for the 24 ensemble member experiments. The increase of ensemble size slightly improves the average RMS errors of the priors of the EnKF and HEnKF for both the IC and ICPH ensembles.

### 5.2 Evaluation of temporal smoothness and insertion noise

To explore the temporal smoothness and potential for insertion noise and dynamic imbalance related to intermittent data assimilation methods, we examine the domain average absolute surface pressure tendency. The magnitude of the surface pressure tendency is often used to quantify model noise in a mesoscale model following data insertion or model initialization (e.g., Chen and Huang 2006). Figure 6 shows the evolutions of the domain average absolute surface pressure tendency for Experiments FDDA, HEnKFIC24, and each ensemble member of Experiment EnKFIC24 and the ensemble mean. It is clear that the EnKF has much higher noise levels than both the FDDA and HEnKF when the three-hourly observations are assimilated, as shown by both the individual ensemble members and the ensemble mean. The noise levels of the EnKF are even higher at the twelve-hourly times when both surface observations and rawinsonde data are assimilated than the other three-hourly times when only surface observations are assimilated. Therefore, the more observations assimilated by the EnKF, the higher the noise level produced by the intermittent EnKF. These spurious high-frequency oscillations decrease quickly with time, but the noise levels of the EnKF are still higher through the 48-h period than those of the FDDA and HEnKF.

It is important to note that the HEnKF, similar to the FDDA but using flow-dependent and time-dependent error covariances from the EnKF, does not show large spikes or discontinuities in surface pressure tendency as the EnKF. These spikes can be greatly reduced by using a digital filter (e.g., Lynch and Huang 1992), but the digital filter can also smooth out physically realistic model-generated high-frequency motions. The HEnKF does not require any digital filtering and shows temporally smooth and better balanced model solutions following the data insertions, which is consistent with the results of applying the HEnKF in the shallow water model (Lei et al. 2011b).

A comparison of the data insertion noise levels for the EnKF and HEnKF when using the 24-member IC ensemble versus the 24-member ICPH ensemble is shown in Fig. 7. The evolution of the ensemble mean of the domain average absolute surface pressure tendencies from Experiment EnKFICPH24 is compared to that of EnKFIC24 in Fig. 7a. The noise levels of the EnKFICPH24 at the three-hourly observation times are even higher than those of the EnKFIC24. However, the noise levels of the HEnKFICPH24 are very similar to those of the HEnKFIC24, as shown by Fig. 7b. Thus adding multi-physics ensemble members increases the already high noise levels of the EnKF, while it has very little impact on the low noise levels of the HEnKF. Similar results are obtained when the ensemble size is increased from 24 to 48 members (not shown). Therefore, the advantages shown in the previous section for the meteorological fields from the HEnKF compared to the EnKF are also accompanied by much lower noise levels following the data assimilation of the HEnKF compared to the EnKF.

### 5.3 Evaluation using independent surface tracer data

An independent verification of the dynamic analyses produced by the set of data assimilation experiments (Table 2) is performed here by comparing the predicted SCIPUFF surface tracer concentrations to the observed CAPTEX-83 surface concentration data. The minimum threshold used for defining "nonzero" concentrations for the predicted and observed surface tracer concentration field is set to 3.0 fl/l (e.g., Lee et al. 2009). This threshold value is three times the minimum value detected by the sensor.

The total numbers of hits, misses and false alarms composited over the 24-h tracer study period for the set experiments are shown in Fig. 8. Overall, the use of Experiment FDDA meteorology fields in SCIPUFF produces the largest number of hits (29) and smallest number of misses (7), while its false alarms were neither the largest nor smallest from the set of experiments. By comparison, Experiment CTRL produces five fewer hits (24) and five more misses (12) than FDDA. Please note that the sum of hits and misses is a constant (one more miss means one fewer hit). Thus only the number of hits and false alarms will be discussed for brevity. Experiment CTRL had 19 false alarms compared to 13 false alarms for FDDA. Note that the statistics for CTRL and FDDA are independent of the ensemble data assimilation experiments group.

For the group of IC24 experiments, Experiment FDDA has six more hits than EnKFIC24, and

5

HEnKFIC24 has three more hits than the EnKFIC24, while EnKFIC24 has one fewer hit than the CTRL. All three data assimilation experiments have fewer false alarms than the CTRL, while the HEnKFIC24 produces the smallest number of false alarms. The better temporal smoothness (better dynamic balance) of the HEnKF dynamic analyses compared to that of the EnKF, as discussed in the previous section, may help to explain why the SCIPUFF using the HEnKF meteorology fields has better statistics from the independent tracer concentration data than the EnKF. This may also contribute to why the FDDA experiment performs so well.

When the additional multi-physics ensemble members are used, the HEnKFICPH24 has five more hits and five fewer false alarms than the EnKFICPH24, while the FDDA has two more hits and one more false alarm than the HEnKFICPH24. The EnKFICPH24 has one fewer hit and three more false alarms than the EnKFIC24. The HEnKFICPH24 has one more hit than the HEnKFIC24, while HEnKFICPH24 has the same number of false alarms as the HEnKFIC24. Therefore, the ICPH ensemble increases the hits (and decreases the misses) with no change of the false alarms for the HEnKF. But the ICPH ensemble degrades all three tracer statistics for the EnKF. The increase in the noise levels in the EnKF caused by the multi-physics ensemble members may contribute to the degradation of the statistics verified against the surface concentration data, because the increased noise levels indicate degraded dynamic consistency.

When the ensemble size is increased from 24 to 48 members, the EnKFIC48 has one more hit than the EnKFIC24, while it has the same number of false alarms as EnKFIC24. The EnKFICPH48 has one fewer hit and one fewer false alarm than the EnKFICPH24. The HEnKFIC48 has one fewer hit and one more false alarm than the HEnKFIC24. The HEnKFICPH48 has one fewer hit and one fewer false alarm than the HEnKFICPH24. Thus there is no clear improvement or degradation for either the EnKF or HEnKF when the ensemble size is increased from 24 to 48. This is consistent with the meteorology statistics and the noise levels that are fairly similar for the same ensemble data assimilation experiments using 24 versus 48 ensemble members. The differences in the meteorological statistics and the noise levels are larger between the IC and ICPH ensembles than those between 24 and 48 ensemble members. The 48-member ICPH ensemble again degrades all three tracer statistics for the EnKF compared to the IC ensemble, which is consistent with the results with 24 ensemble members. However, the ICPH ensemble with 48 members increases the hits, and decreases the false alarms for the HEnKF compared to the IC ensemble.

To assess the overall performance of each data assimilation method verified against the surface tracer data, we assign an ordinal ranking to the set of experiments in Table 4. The rank is based on the sum of misses and false alarms in the 24-h tracer study period. Since the sum of hits and misses is a constant, the hits are already represented by the value of misses.

By looking for smaller values of the sum of misses and false alarms, we can define the better performing experiments in terms of the tracer verification. Experiment FDDA has the smallest value of the sum (20), while Experiment HEnKF with the 24-member or 48-member ICPH ensemble (HEnKFICPH24 or HEnKFICPH48) has a value only one larger than that of the FDDA. The HEnKF with the 24-member and 48-member IC ensemble (HEnKFIC24 and HEnKFIC48) has values of 22 and 24, respectively. All HEnKF experiments produce smaller values of the sum than the EnKF experiments. The best EnKF experiment, EnKFIC48, shows a value of 26, followed by EnKFIC24 with 27, and these sums are five or six larger than that of the best HEnKF experiment (HEnKFICPH24 or HEnKFICPH48). Finally, Experiments EnKFICPH24, EnKFICPH48 and CTRL show a value of 31, and this value is at least 10 larger than those at or near the top of the list, Experiments FDDA and HEnKFICPH24 / HEnKFICPH48.

Although this independent verification is for only one case with a limited sample, the results are consistent. The experiments having good posteriors and priors along with low insertion noise scored higher with the independent tracer data. There appears to be some advantage in the hourly analyses produced by the continuous HNEnKF compared to the intermittent EnKF. This is also consistent with the lower noise levels of Experiment HEnKF compared to the Experiment EnKF in the previous section. Therefore, the added value of the HNEnKF, which applies the EnKF gradually in time via nudging-type terms and produces better temporal smoothness, has been demonstrated.

## 6. Conclusions

A hybrid nudging-EnKF (HNEnKF) data assimilation approach was proposed and tested in Lei et al. (2011a, b), and it is investigated here using WRF/DART with real observations from the CAPTEX-83 case. The HNEnKF effectively combines the strengths of the EnKF and nudging while avoiding their individual weaknesses. It applies the EnKF gradually in time via nudging-type terms, and provides flow-dependent and time-dependent nudging coefficients by using the EnKF. The HNEnKF also extends the nudging coefficients to include nonzero off-diagonal elements, which improves the inter-variable influences of the innovations and dynamic consistency.

The set of data assimilation methods is first verified against the meteorological data. For the 24-member IC ensemble based on perturbations of the ICs and LBCs, the HNEnKF has better fit-to-observation statistics (posterior) than the EnKF for both wind and mass fields, although both HNEnKF and EnKF have larger posterior RMS errors than the FDDA. The HNEnKF has similar or better three-hourly forecast (prior) statistics than the EnKF and FDDA. The 24-member ICPH ensemble improves the posteriors and slightly improves the priors of the mass fields compared to the IC ensemble for the EnKF and HNEnKF, with larger improvements for the EnKF. The wind field posteriors and priors are very

similar for the IC and ICPH ensembles. The increase of ensemble size from 24 to 48 slightly improves the posteriors and priors of the EnKF and HNEnKF for wind and mass for both the IC and ICPH ensembles. The comparisons between EnKF and HNEnKF for both the IC and ICPH ensembles of 48 ensemble members are consistent with those of the 24 ensemble members.

The analyses of the domain average absolute surface pressure tendency shows that the intermittent EnKF has much higher noise levels than the continuous HNEnKF and FDDA approaches when three-hourly observations are assimilated. The noise levels in the EnKF are even higher at the twelve-hourly times when rawinsonde data are also assimilated and when multi-physics ensemble members are included, while the HNEnKF shows little sensitivity to these factors. This demonstrates that the HNEnKF is able to provide better temporal smoothness and dynamic consistency in the hourly analyses than the EnKF while retaining its advantages by using the flow-dependent and time-dependent background error covariances to spread the innovations in the horizontal and vertical directions.

Finally, the set of data assimilation methods is verified against the independent surface tracer data. The FDDA has the best overall statistics, as represented by the smallest value of the sum of misses and false alarms, followed by the HNEnKF using the ICPH ensemble and having a value only one larger than that of the FDDA. The HNEnKF produces consistently better statistics than the EnKF. Compared to the IC ensemble, the ICPH ensemble decreases the misses without increasing the false alarms for the HNEnKF, but the ICPH ensemble degrades all tracer data statistics for the EnKF. Because the HNEnKF analyses used to drive the SCIPUFF produce consistently better tracer data verification statistics than the EnKF, there appears to be some advantage in the dynamic analyses produced by the continuous HNEnKF compared to the intermittent EnKF, as we hypothesized using simple models and OSSEs in Lei et al. (2001a, b).

**Acknowledgements**

**References**

Anderson J. L., 2001: An ensemble adjustment Kalman filter for data assimilation. *Mon. Wea. Rev.*, **129**, 2884-2903.

Anderson J. L., 2007: An adaptive covariance inflation error correction algorithm for ensemble filters. *Tellus*, **59A**, 210-224.

Anderson, J. L., T. Hoar, K. Raeder, N. Collins, R. Torn, A. F. Arellano, 2009: The Data Assimilation Research Testbed: A community data assimilation facility. *Bull. Amer. Meteor. Soc.*, **90**, 1283-1296

Baker, D. M., W. Huang, Y.-R. Guo, A. Bourgeois, and Q. N. Xiao, 2004: A three-dimensional variational data assimilation system for MM5: Implementation and initial results. *Mon. Wea. Rev.,* **132**, 897-914.

Benjamin, S. G., and N. L. Seaman, 1985: A simple scheme for objective analysis in curved flow. *Mon. Wea. Rev.*, **113**, 1184-1198.

Betts, A. K., and M. J. Miller, 1986: A new convective adjustment scheme. Part II: Single column tests using GATE wave, OBMEX, and arctic air-mass data sets. *Quart. J. Roy. Meteor. Soc.*, **112**, 693-709.

Chen, M., and X. Huang, 2006: Digital filter initialization for MM5. *Mon. Wea. Rev.,* **134**, 1222-1236.

Deng, J., N. L. Seaman, G. K. Hunter, and D. R. Stauffer, 2004: Evaluation of interregional transport using the MM5-SCIPUFF system. *J. Appl. Meteor.*, **43**, 1864-1886.

Deng, J., and D. R. Stauffer, 2006: On improving 4-km mesoscale model simulations. *J. Appl. Meteor.*, **45**, 361-381.

Deng, A., D.R. Stauffer, B. Gaudet, J. Dudhia, C. Bruyere, W. Wu, F. Vandenberghe, Y. Liu, and A. Bourgeois, 2009: Update on WRF-ARW end-to-end multi-scale FDDA system, Preprint, *WRF Users' Workshop*, Boulder, CO, June 23-26.

Dudhia, J., 1989: Numerical study of convection observed during the winter monsoon experiment using a mesoscale two-dimensional model. *J. Atmos. Sci.*, 46, 3077-3107.

Evensen, G., 1994: Sequential data assimilation with a nonlinear quasi-geostrophic model using Monte Carlo methods to forecast error statistics. *J. Geophys. Res.*, **99(C5)**, 10143-10162.

Gaspari, G., and S. E. Cohn, 1999: Construction of correlation functions in two and three dimensions. *Quart. J. Roy. Meteor. Soc.*, **125**, 723-757.

Hong, S-.Y., J. Dudhia, S. -H. Chen, 2004: A revised approach to ice-microphysical processes for the bulk parameterization of cloud and precipitation. *Mon. Wea. Rev.*, **132**, 103-120.

Hong, S-.Y., Y. Noh, and J. Dudhia, 2006: A new vertical diffusion package with an explicit treatment of entrainment processes. *Mon. Wea. Rev.*, **134**, 2318-2341.

Houtekamer, P. L., and H. L. Mitchell, 1998: Data assimilation using an ensemble Kalman filter technique. *Mon. Wea. Rev.*, **126**, 796-811.

Janjić, Z. I., 1994: The step-mountain eta coordinate model: Further developments of the convection, viscous sublayer, and turbulence closure schemes. *Mon. Wea. Rev.*, 122, 927-945.

Kain, J. S., and J. M. Fritsch, 1990: A one-dimensional entraining / detraining plume model and its application in convective parameterization. *J. Atmos. Sci.*, 47, 2784-2802.

Lei, L., D. R. Stauffer, S. E. Haupt, and G. S. Young, 2011a: A hybrid nudging-ensemble Kalman filter approach to data assimilation. Part I: Application in the Lorenz system. *Submitted to Tellus.*

Lei, L., D. R. Stauffer, and A. Deng, 2011b: A hybrid nudging-ensemble Kalman filter approach to data assimilation. Part II: Application in a shallow-water model. *Submitted to Tellus.*

Lee, J. A., L. J. Peltier, S. E. Haupt, J. C. Wyngaard, D. R. Stauffer, and A. Deng, 2009: Improving SCIPUFF dispersion forecasts with NWP ensembles. *J. Appl. Meteor. Climatol,* **48**, 2305-2319.

Lin, Y.-L., R. D. Farley, and H. D. Orville, 1983: Bulk parameterization of the snow field in a cloud model. *J. Climate Appl. Meteor.*, **22**, 1065-1092.

Lynch, P., and X.-Y. Huang, 1992: Initialization of the HIRLAM model using a digital filter. *Mon. Wea. Rev.*, **125**, 655-660.

Mlawer, E. J., S. J. Taubman, P. D. Brown, M. J. Iacono, and S. A. Clough, 1997: Radiative transfer for inhomogeneous atmosphere: RRTM, a validated correlated-k model for the long-wave. *J. Geophys. Res.*, **102**(D14), 16663-16682.

Rogers, R., A. Deng, D. R. Stauffer, Y. Jia, S.-T. Soong, S. Tanrikulu, S. Beaver, and C. Tran, 2011: Fine particulate matter modeling in Central California. Part I: Application of the Weather Research and Forecasting model. *In 91th Annual Meeting.* American Meteorological Society: Seattle, WA, p 5.3.

Schroeder, A.J., D.R. Stauffer, N.L. Seaman, A. Deng, A.M. Gibbs, G.K. Hunter and G.S. Young, 2006: Evaluation of a high-resolution, rapidly relocatable meteorological nowcasting and prediction system. *Mon. Wea. Rev.*, **134**, 1237-1265.

Skamarock, W. C., J. B. Klemp, J. Dudhia, D. O. Gill, D. M. Barker, M. Duda, X.-Y. Huang, W. Wang and J. G. Powers, 2008: A description of the advanced research WRF version 3, NCAR Tech Note, 125 pp. [Available from UCAR communications, P. O. Box 3000, Boulder, CO, 80307; online at: http://www.mmm.ucar.edu/wrf/users/docs/arw_v3.pdf]

Snyder, C., T. Bengtsson, P. Bickel, and J. Anderson, 2008: Obstacles to high-dimensional particle filtering. *Mon. Wea. Rev.*, 136, 4629-4640.

Stauffer, D. R., and N. L. Seaman, 1990: Use of four-dimensional data assimilation in a limited-area mesoscale model. Part I: Experiments with synoptic data. *Mon. Wea. Rev.,* **118**, 1250-1277.

Stauffer, D. R., and N. L. Seaman, 1994: Multiscale four-dimensional data assimilation. *J. Appl. Meteor.,* **33**, 416-434.

Sykes, R. I., S. F. Parker, and D. S. Henn, 2004: SCIPUFF version 2.0, technical documentation. A.R.A.P. Tech. Rep. 727, Titan Corporation, Princeton, NJ, 284pp.

Table 1.  Eight different physics configurations for the ICPH ensemble.  The first physics configuration is the default physics configuration used in the IC ensemble.

| Physics configuration | Microphysics | Convective | PBL |
|---|---|---|---|
| 1 | WSM-3 | Kain-Fritsch | MYJ |
| 2 | Lin et al. | Kain-Fritsch | MYJ |
| 3 | WSM-3 | Betts-Miller-Janjic | MYJ |
| 4 | WSM-3 | Kain-Fritsch | YSU |
| 5 | Lin et al. | Betts-Miller-Janjic | MYJ |
| 6 | Lin et al. | Kain-Fritsch | YSU |
| 7 | WSM-3 | Betts-Miller-Janjic | YSU |
| 8 | Lin et al. | Betts-Miller-Janjic | YSU |

Table 2.  Experiment design of the HNEnKF in WRF / DART.

| Exp. Name | Exp. Description |
|---|---|
| CTRL | Assimilate no observations |
| FDDA | Assimilate observations by observation nudging |
| EnKFIC24 | Assimilate observations by EnKF with IC ensemble and 24 ensemble members |
| EnKFIC48 | Assimilate observations by EnKF with IC ensemble and 48 ensemble members |
| EnKFICPH24 | Assimilate observations by EnKF with ICPH ensemble and 24 ensemble members |
| EnKFICPH48 | Assimilate observations by EnKF with ICPH ensemble and 48 ensemble members |
| HEnKFIC24 | Assimilate observations by HNEnKF with IC ensemble and 24 ensemble members |
| HEnKFIC48 | Assimilate observations by HNEnKF with IC ensemble and 48 ensemble members |
| HEnKFICPH24 | Assimilate observations by HNEnKF with ICPH ensemble and 24 ensemble members |
| HEnKFICPH48 | Assimilate observations by HNEnKF with ICPH ensemble and 48 ensemble members |

Table 3. Major data assimilation parameters for the set of experiments.  See section 3.4 for details.

| Experiment | Nudging strength | Horizontal radius of influence | Surface data vertical radius of influence (stable PBL) | Surface data vertical radius of influence (unstable PBL) | Half-period of nudging time window | Horizontal error covariance localization | Vertical error covariance localization | Error covariance inflation |
|---|---|---|---|---|---|---|---|---|
| FDDA | $4\times10^{-4}$ $s^{-1}$ | 67-200 km | 100 m | PBL top plus 50m | 1-2 h | --- | --- | --- |
| EnKF | --- | --- | --- | --- | --- | 533 km | 150 hPa | Adaptive inflation |
| HEnKF | --- | --- | --- | --- | 1-2 h | 533 km | 150 hPa | Adaptive inflation |

Table 4.  Ordinal ranking of the set of experiments by the sum of misses and false alarms from the independent tracer data verification.

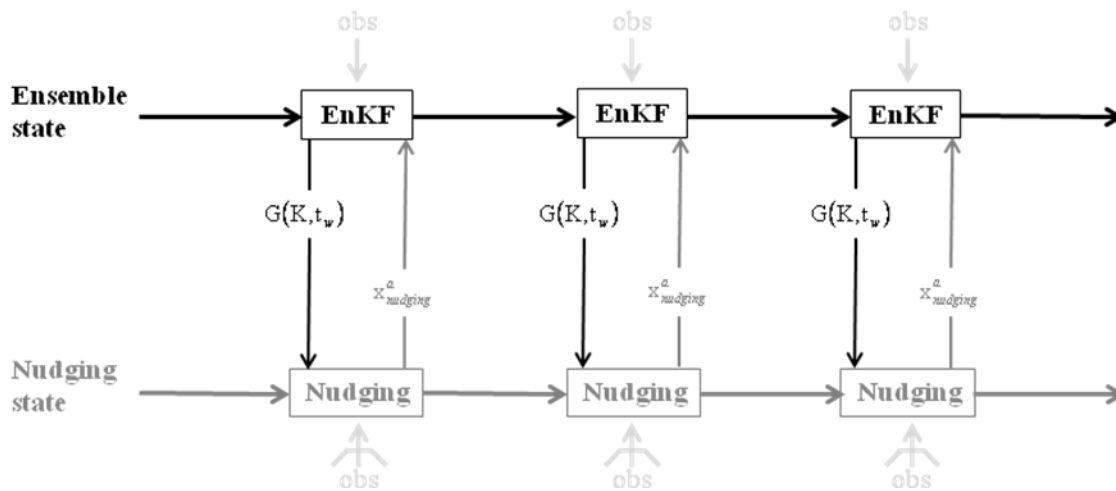| Ordinal ranking | Experiment | Sum of misses and false alarms |
|---|---|---|
| 1 | FDDA | 20 |
| 2 | HEnKFICPH24 | 21 |
| 2 | HEnKFICPH48 | 21 |
| 3 | HEnKFIC24 | 22 |
| 4 | HEnKFIC48 | 24 |
| 5 | EnKFIC48 | 26 |
| 6 | EnKFIC24 | 27 |
| 7 | EnKFICPH24 | 31 |
| 7 | EnKFICPH48 | 31 |
| 7 | CTRL | 31 |

Figure 1. Schematic showing the procedures of the hybrid nudging-EnKF approach (after Lei et al. 2011a).



Figure 2. The WRF 12-km domain (outer domain) and the 12-km SCIPUFF domain (inner domain).
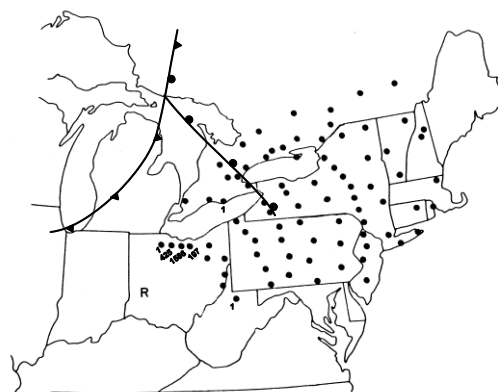


Figure 3. Surface cold and warm fronts during CAPTEX at 2200 UTC 18 September 1983. Observed tracer concentrations (parts of perflurocarbon per $10^{15}$ parts of air by volume, or femtoliters/liter) at this time are shown over the surface sampling network (after Deng et al. 2004). "R" is the release point at Dayton, OH.
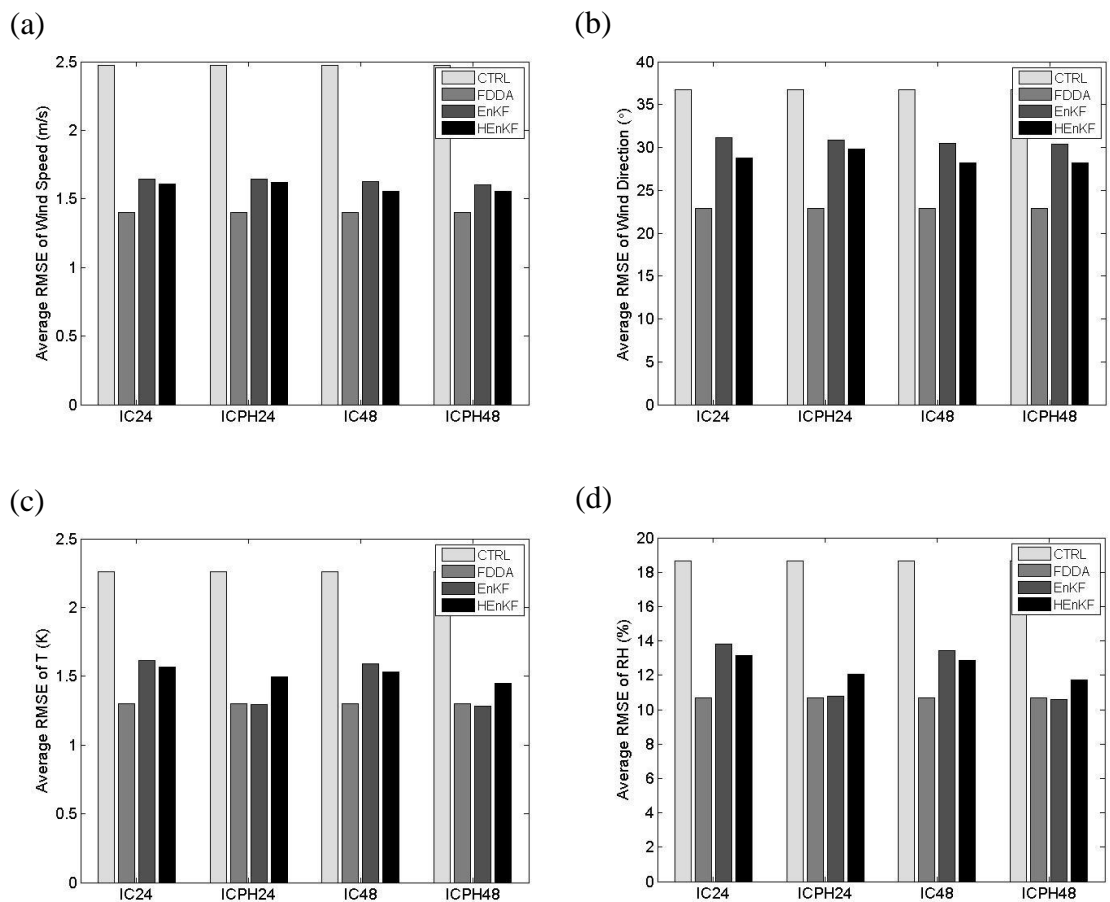
(a)



(b)



(c)



(d)



Figure 4. The average RMS errors of the posteriors for Experiments CTRL and FDDA, and Experiments EnKF and HEnKF for both IC and ICPH ensembles with 24 or 48 ensemble members through the 48-h simulation period. (a) wind speed (ms$^{-1}$), (b) wind direction (degrees), (c) temperature (K) and (d) relative humidity (percent).
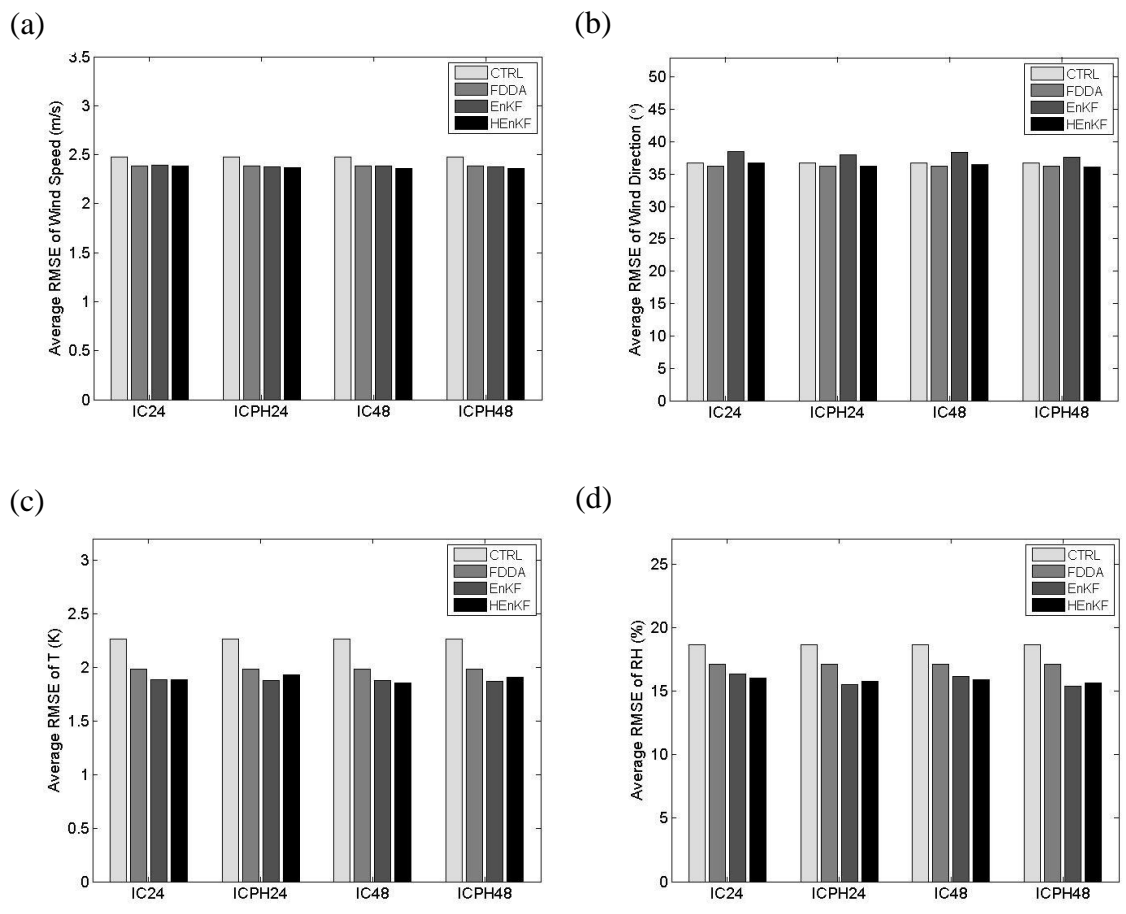
(a)

(b)

(c)

(d)

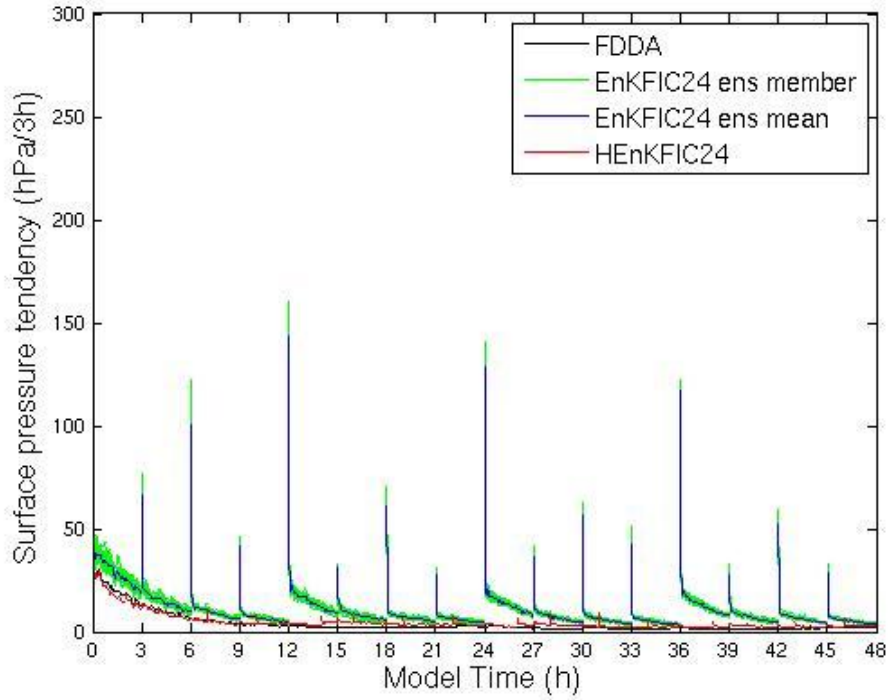Figure 5.  The same as Fig. 4, except for the priors.

13

Figure 6. The evolutions of the domain average absolute surface pressure tendency of Experiment FDDA, each ensemble member of Experiment EnKFIC24 and their ensemble mean, and Experiment HEnKFIC24.
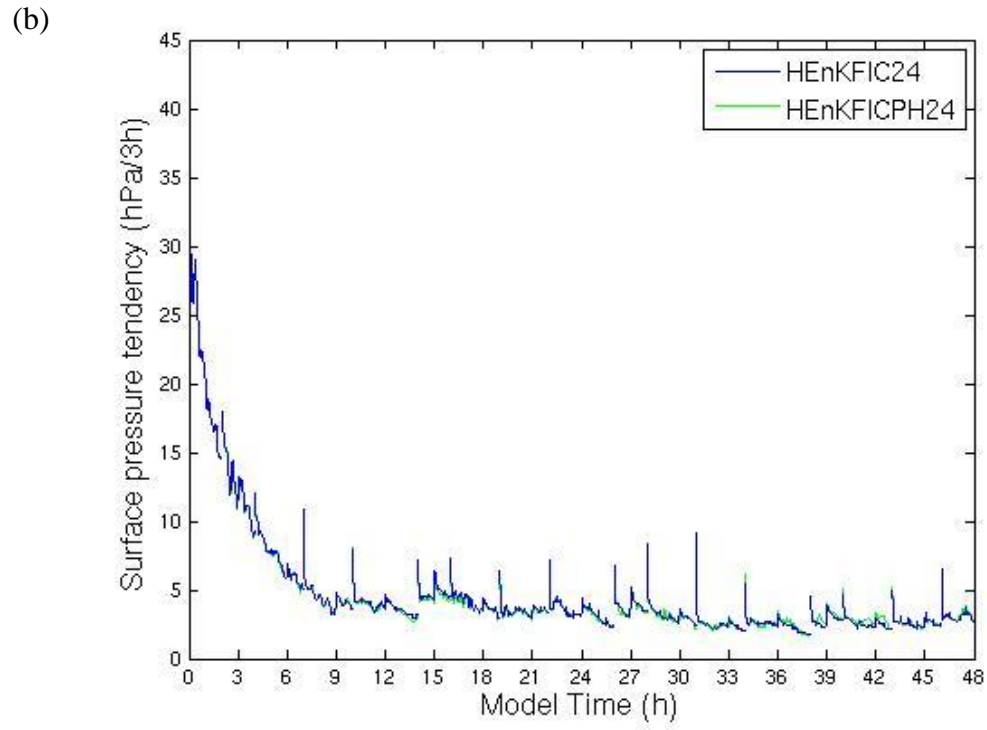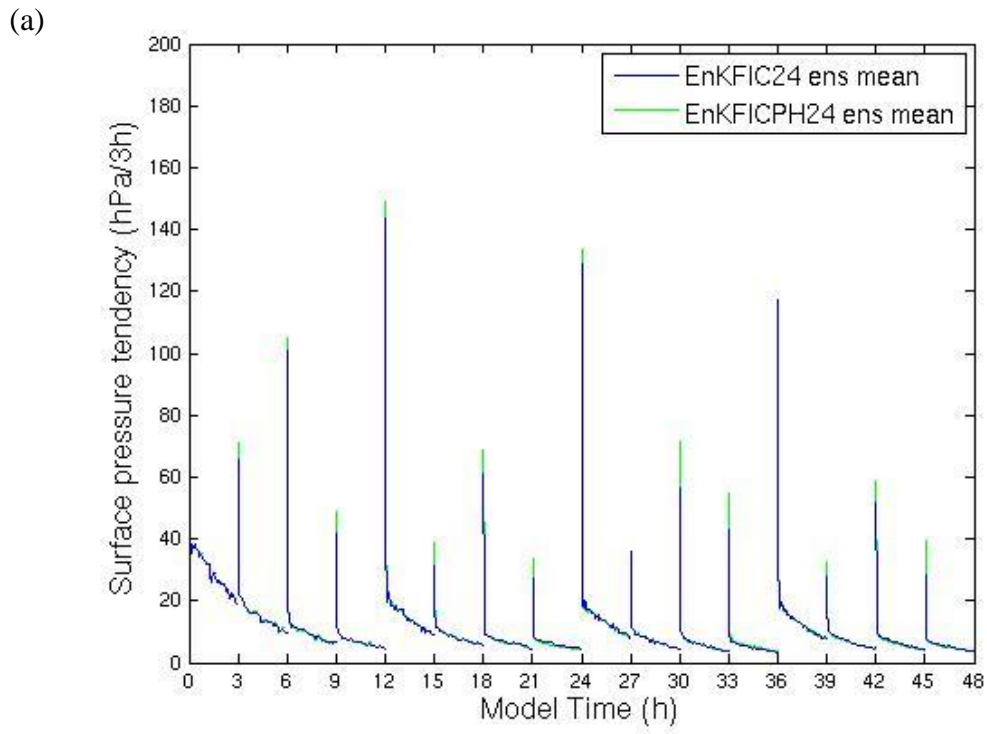
(a)



(b)



Figure 7. The evolutions of the domain average surface pressure tendencies. (a) ensemble mean of Experiments EnKFIC24 and EnKFICPH24, and (b) Experiments HEnKFIC24 and HEnKFICPH24.

15

**Total**

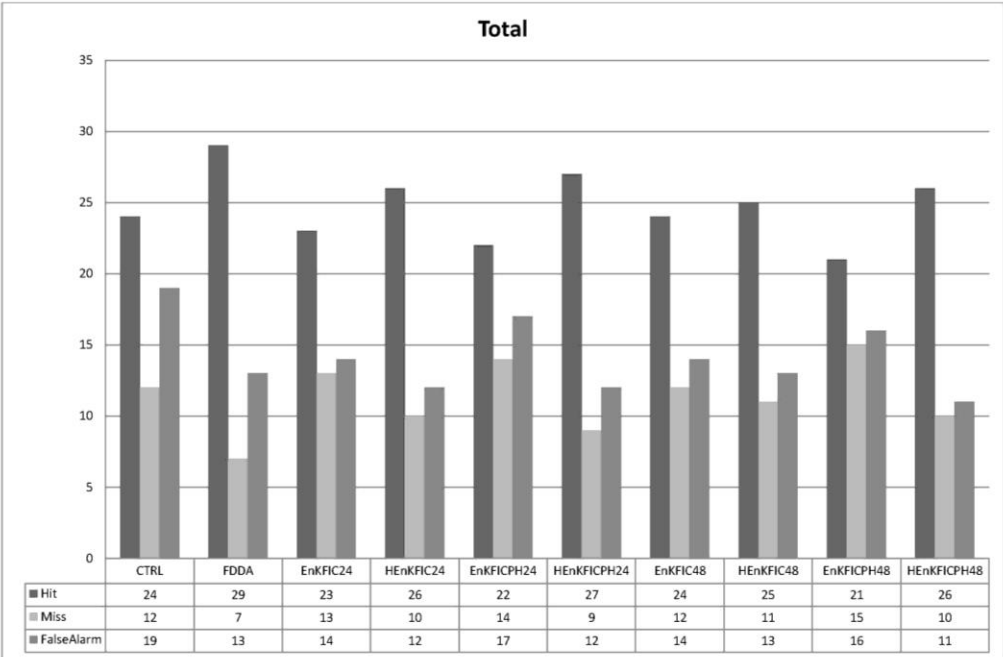| | CTRL | FDDA | EnKFIC24 | HEnKFIC24 | EnKFICPH24 | HEnKFICPH24 | EnKFIC48 | HEnKFIC48 | EnKFICPH48 | HEnKFICPH48 |
|---|---|---|---|---|---|---|---|---|---|---|
| Hit | 24 | 29 | 23 | 26 | 22 | 27 | 24 | 25 | 21 | 26 |
| Miss | 12 | 7 | 13 | 10 | 14 | 9 | 12 | 11 | 15 | 10 |
| FalseAlarm | 19 | 13 | 14 | 12 | 17 | 12 | 14 | 13 | 16 | 11 |

Figure 8. The composite statistics (hits, misses and false alarms) of the predicted surface tracer concentration through the 24-h period from each experiment from Table 2 verified against the observed surface tracer concentration data.